

Exohiss wave enhancement following substorm electron injection in the dayside magnetosphere

ZhongLei Gao^{1,2,3,4}, ZhenPeng Su^{2,3*}, FuLiang Xiao¹, HuiNan Zheng^{2,3}, YuMing Wang², Shui Wang², H. E. Spence⁵, G. D. Reeves^{6,7}, D. N. Baker⁸, J. B. Blake⁹, and H. O. Funsten¹⁰

¹School of Physics and Electronic Sciences, Changsha University of Science and Technology, Changsha 410004, China;

²CAS Key Laboratory of Geospace Environment, Department of Geophysics and Planetary Sciences, University of Science and Technology of China, Hefei, Anhui 230026, China;

³Collaborative Innovation Center of Astronautical Science and Technology, University of Science and Technology of China, Hefei 230026, China;

⁴Mengcheng National Geophysical Observatory, School of Earth and Space Sciences, University of Science and Technology of China, Hefei 230026, China;

⁵Institute for the Study of Earth, Oceans, and Space, University of New Hampshire, Durham, New Hampshire, USA;

⁶Space Science and Applications Group, Los Alamos National Laboratory, Los Alamos, New Mexico, USA;

⁷Space Sciences Division, New Mexico Consortium, Los Alamos, New Mexico, USA;

⁸Laboratory for Atmospheric and Space Physics, University of Colorado Boulder, Colorado, USA;

⁹The Aerospace Corporation, Los Angeles, California, USA;

¹⁰ISR Division, Los Alamos National Laboratory, Los Alamos, New Mexico, USA

Abstract: Exohiss is a low-frequency structureless whistler-mode emission potentially contributing to the precipitation loss of radiation belt electrons outside the plasmasphere. Exohiss is usually considered the plasmaspheric hiss leaked out of the dayside plasmapause. However, the evolution of exohiss after the leakage has not been fully understood. Here we report the prompt enhancements of exohiss waves following substorm injections observed by Van Allen Probes. Within several minutes, the energetic electron fluxes around 100 keV were enhanced by up to 5 times, accompanied by an up to 10-time increase of the exohiss wave power. These substorm-injected electrons are shown to produce a new peak of linear growth rate in the exohiss band ($< 0.1f_{ce}$). The corresponding path-integrated growth rate of wave power within 10° latitude of the magnetic equatorial plane can reach 13.4, approximately explaining the observed enhancement of exohiss waves. These observations and simulations suggest that the substorm-injected energetic electrons could amplify the preexisting exohiss waves.

Keywords: exohiss; substorm injection; radiation belt; whistler-mode instability

Citation: Gao Z. L., Su Z. P., Xiao F. L., Zheng H. N., Wang Y. M., Wang S., Spence H. E., Reeves G. D., Baker D. N., Blake J. B., and Funsten H. O. (2018). Exohiss wave enhancement following substorm electron injection in the dayside magnetosphere. *Earth Planet. Phys.*, 2(5), 359–370. <http://doi.org/10.26464/epp2018033>

1. Introduction

Wave-particle interaction is one of the most important mechanisms controlling the radiation belt dynamics (see review by Thorne, 2010). In particular, two types of whistler-mode waves, chorus and plasmaspheric hiss, are frequently invoked to explain the acceleration and loss of radiation belt electrons (e.g., Abel and Thorne, 1998; Horne and Thorne, 1998; Summers et al., 1998, 2002; Horne et al., 2005; Shprits et al., 2006; Artemyev et al., 2012; Thorne et al., 2013; Ni BB et al., 2014; Su ZP et al., 2014a, 2016; Gao ZL et al., 2016; Yang C et al., 2016). The generation/evolution of the two types of whistler-mode waves has been studied extensively. The substorm-injected anisotropic energetic (from a few keV

to tens of keV) electrons outside the plasmasphere are believed to provide the free energy of chorus (e.g., Kennel and Engelmann, 1966; Li W et al., 2009; Su ZP et al., 2014b); the discrete frequency-time structures (e.g., Santolík et al., 2014) of chorus are usually considered a result of the nonlinear cyclotron resonance (e.g., Nunn et al., 1997; Omura et al., 2008). For plasmaspheric hiss, the candidate generation mechanisms include: (1) origination from lightning whistlers in the plasmasphere (e.g., Sonwalkar and Inan, 1989; Green et al., 2005), (2) excitation by electron cyclotron instability in the outer plasmasphere (Thorne et al., 1979; Li W et al., 2013; Chen LJ et al., 2014; Summers et al., 2014), and (3) origination from chorus outside the plasmasphere (Bortnik et al., 2008, 2009; Su ZP et al., 2015; Liu NG et al., 2017).

In fact, there exists another type of whistler-mode wave, named exohiss, outside the plasmasphere (Russell et al., 1969; Thorne et al., 1973; Solomon et al., 1988; Kurth and Gurnett, 1991; Golden et al., 2009, 2011). Different from the normal (Santolík et al., 2002,

Correspondence to: Z. P. Su, szpe@mail.ustc.edu.cn

Received 05 JUL 2018; Accepted 27 AUG 2018.

Accepted article online 06 SEP 2018.

©2018 by Earth and Planetary Physics.

2003b) and low-frequency (Cattell et al., 2015; Gao ZL et al., 2016) chorus waves propagating away from the equator, exohiss waves usually exhibit the equatorward or bi-directional Poynting fluxes (Zhu H et al., 2015). Recently, it has been suggested that exohiss waves may cause precipitation loss of radiation belt electrons (Zhu H et al., 2015). In contrast to the significant progress made in understanding the generation/evolution of chorus and plasmaspheric hiss, quite limited attention has been paid to exohiss generation/evolution. In view of the frequent occurrence of exohiss in the dayside high-latitude region, Thorne et al. (1973) suggested that exohiss could be plasmaspheric hiss leaking from the plasmasphere. Such a generation scenario of exohiss has been supported by full-time raytracing simulations (Bortnik et al., 2008). However, until now, the evolution of exohiss outside the plasmasphere has not been fully understood. Here, on the basis of the Van Allen Probes (Mauk et al., 2013) observations and the linear instability theory (Kennel, 1966), we show that exohiss can be amplified significantly by substorm-injected energetic electrons.

2. Data and Methods

The twin Van Allen Probes reside in elliptical orbits to understand the fundamental physics of the radiation belts (Mauk et al., 2013). We mainly use the data sets from the Electric and Magnetic Field Instrument and Integrated Science (EMFISIS) suite (Kletzing et al., 2013) and the Energetic Particle, Composition and Thermal Plasma Suite (ECT) (Spence et al., 2013). The local magnetic field was observed with a 64 Hz sample rate by the tri-axial fluxgate magnetometer (MAG) of the EMFISIS suite. The corresponding ratio of the local magnetic field to the equatorial field is approximately modeled by the TS04 package (Tsyganenko and Sitnov, 2005). The cold electron density is derived from the upper hybrid resonance frequency measured by the High Frequency Receiver (HFR) of the EMFISIS Waves instrument (Kurth et al., 2014). Wave spectral matrices with a time resolution of 6 s in survey mode and waveforms sampled in burst mode at a rate of 35 kHz are provided by the Waveform receiver (WFR) of the EMFISIS Waves instrument. A 70%-overlapped, 1024-point fast Fourier transform (FFT) is performed on the waveform data to obtain the wave spectral matrices in the burst mode. The singular value decomposition method (Santolík et al., 2002, 2003a, 2010) is used on these spectral matrices (in the survey and burst modes) to determine the wave normal angle, ellipticity, planarity, and Poynting vector. The electron differential fluxes in the energy range from 15 eV to 4 MeV were detected by the Helium, Oxygen, Proton, and Electron (HOPE) Mass Spectrometer (Funsten et al., 2013) and by the Magnetic Electron Ion Spectrometer (MagEIS) (Blake et al., 2013) of the ECT suite.

We use a recently developed code (Liu NG et al., 2018a, b; Su ZP et al., 2018) to analyze the linear instability (Kennel, 1966) of whistler waves; this analysis does not take into account relativistic effects. Summers et al. (2009) conclude that linear growth rates are not significantly affected by ignoring relativistic effects. The temporal growth rate γ and the convective growth rate K_i can be expressed as

$$\gamma = \frac{-D_i}{\partial D^0 / \partial \omega}, \quad (1)$$

$$K_i = \gamma / |\mathbf{V}_g|, \quad (2)$$

where D^0 and D_i are the real and imaginary parts of the dispersion relation $D(\omega, k, \psi) = D^0 + iD_i$ (Chen LJ et al., 2010, equations (A3)) with angular frequency ω , wave normal angle ψ , and wave number $k = k \cos \psi \mathbf{e}_\parallel + k \sin \psi \mathbf{e}_\perp$. The electron phase space density and its partial derivative with respect to the velocity vector are required to calculate D_i (Chen LJ et al., 2010, equations (A4)). Those fitting parameters for the electron phase space density are specified in the following sections.

3. Event on 21 February 2014

3.1 Observation

Figure 1 gives an overview of the exohiss enhancement event observed by the twin Van Allen Probes in the time range 06:00–12:00 UT on 21 February 2014. During this time range, the magnetosphere was experiencing a moderate storm ($SYM-H \sim 50$ nT) and some moderate substorms ($AE > 600$ nT). A steep density gradient in the plasmapause was detected by Van Allen Probe A around 06:50 UT and by Van Allen Probe B around 11:30 UT. There existed plasmaspheric hiss (0.1–2 kHz) inside the plasmasphere but chorus (0.1–0.5 f_{ce}) and exohiss (0.1–0.4 kHz) outside the plasmasphere (Here f_{ce} represents the equatorial electron gyro-frequency). The three types of whistler-mode waves were right-hand polarized with ellipticity values >0.7 , but had distinct characteristics of normal angle, planarity, and Poynting flux direction. Due to bounce propagation in the plasmasphere, plasmaspheric hiss waves had low values of planarity, broadly distributed wave normal angles (30° – 70°), and nearly randomly distributed Poynting flux directions. Chorus waves possessed small wave normal angles ($< 20^\circ$), large planarity values (> 0.7) and negative Poynting fluxes, indicating their equatorial generation and poleward propagation. Exohiss waves exhibited small wave normal angles ($< 30^\circ$) and moderate planarity values (0.5–0.8). The Poynting flux direction of exohiss appeared to be dependent on magnetic latitude and wave frequency (Zhu H et al., 2015). Around the most negative latitudes ($-17^\circ < MLAT < -14^\circ$), exohiss waves were dominated by equatorward propagations. As the twin probes moved toward the equator, the expanding high-frequency part of exohiss showed poleward propagations. These observations imply the leakage of plasmaspheric hiss from both the Northern and Southern Hemispheres of the plasmasphere. Compared to plasmaspheric hiss, exohiss had an up to 2 orders of magnitude lower power spectral density. A substorm injection arrived at Probe A around 09:30 UT; about five minutes later, Probe B also encountered the substorm injection. During the time period of the substorm injection, both probes were in the dayside ($MLT \sim 12:00$ – $13:00$) southern hemisphere ($MLAT < -10^\circ$) at $L \sim 6$. The fluxes of injected electrons in the energy-time domain were wedge-shaped resulting from the energy-dependent azimuthal drift of electrons. The upper energy cut-offs of the substorm injection were ~ 200 keV, and the corresponding minimum cyclotron resonant frequencies were 0.1–0.3 kHz (depending on L -shell). The substorm injection promptly enhanced the exohiss wave power detected by both probes. For Probe A, there was a 10 times enhancement of exohiss power and the enhanced exohiss and chorus bands merged after the substorm injection. For Probe B, the exohiss wave power increased

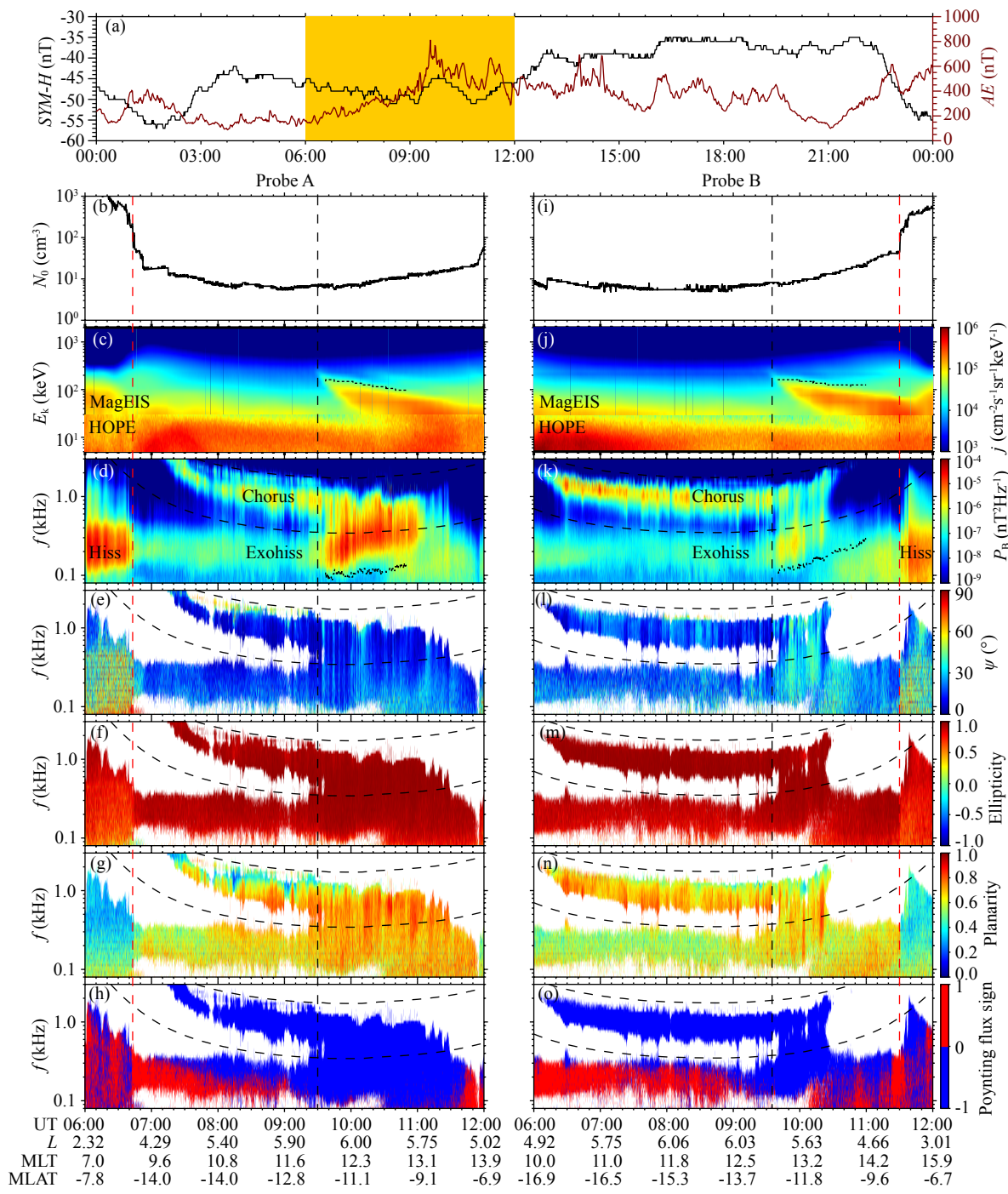


Figure 1. Exohiss amplification event recorded by Van Allen Probes A (left) and B (right) on 21 February 2014. (a) Geomagnetic activity indices AE and $SYM-H$ with the yellow shadow marking the interval of interest; (b, i) Cold electron density; (c, j) Electron differential flux; (d, k) Wave magnetic power spectral density; (e, l) Wave normal angle; (f, m) Wave ellipticity; (g, n) Wave planarity and (h, o) sign of Poynting flux parallel to background magnetic field (positive value for northward direction and negative value for southward direction). Dotted lines in Figures 1c and 1j denote the upper energy cut-off of the substorm, and dotted lines in Figures 1d–1h and 1k–1o represent $0.1f_{ce}$ and $0.5f_{ce}$. The vertical red and black lines mark the location of the plasmapause and the arrival time of the substorm injection, respectively. The normal angle, ellipticity, planarity and Poynting direction are shown only for the corresponding power spectral densities $P_B > 5 \times 10^{-8} \text{ nT}^2 \text{Hz}^{-1}$.

less than 5 times and a gap with a minimum of wave power between exohiss and chorus bands existed all the time.

Figures 2 and 3 show the wave fine structure observed by two probes before and after the substorm injection. In the frequency-

time spectra, the pre-injection chorus and exohiss were basically split in frequency by $0.1f_{ce}$. After the substorm injection, the wave power spectral densities over a wide frequency range were enhanced obviously but no significant changes in wave fine struc-

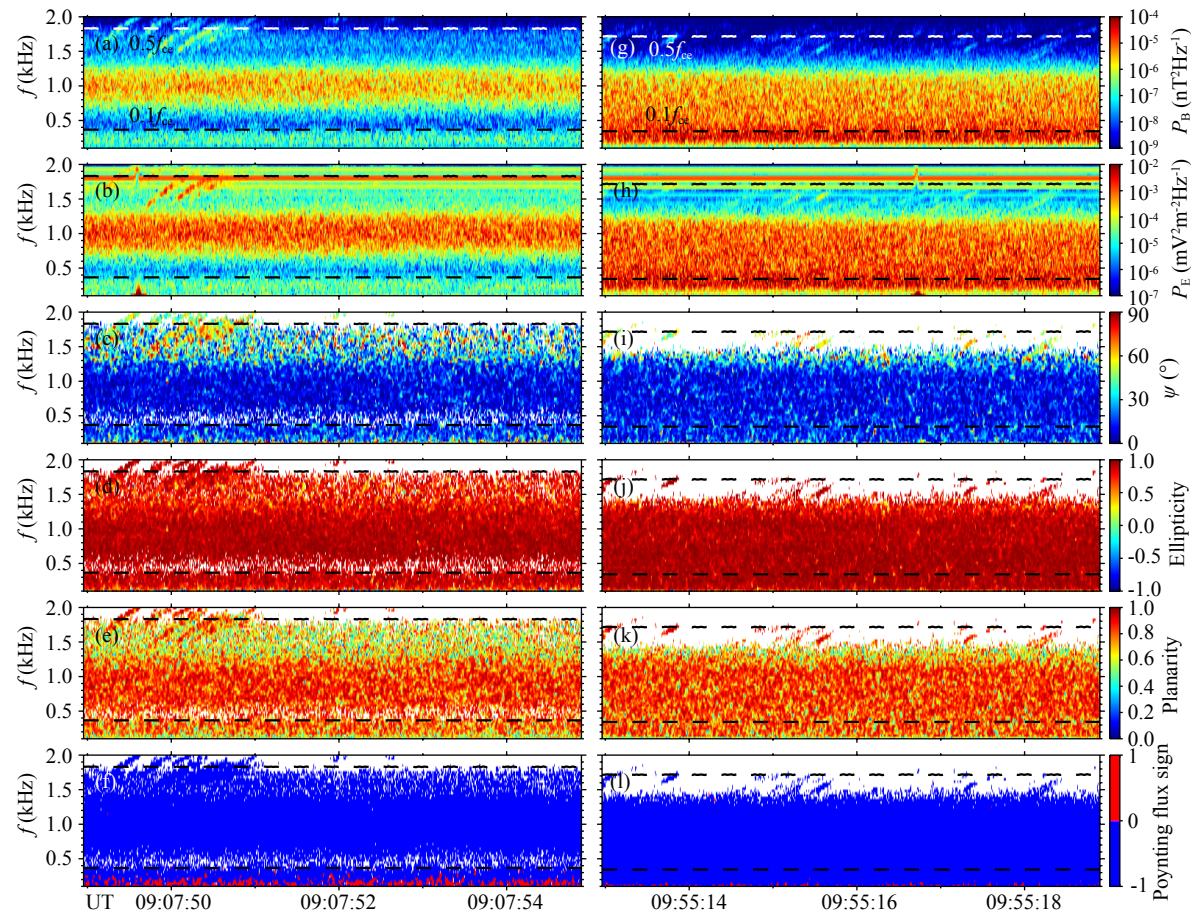


Figure 2. (a–f) Pre-substorm and (g–l) post-substorm wave fine structure recorded by Van Allen Probe A. (a, b, g, h) Power spectral density; (c, i) Wave normal angle; (d, j) Ellipticity; (e, k) Planarity, and (f, l) sign of Poynting flux parallel to background magnetic field. The dashed lines in each panel represent the frequency of 0.1 and $0.5f_{ce}$. The normal angle, ellipticity, planarity and Poynting direction are only shown for the corresponding power spectral densities $P_B > 10^{-8} \text{ nT}^2 \text{Hz}^{-1}$.

ture occurred. Throughout the event, exohiss emission appeared as a noisy band, while chorus emission consisted of a noisy band and some sporadic rising tones. Different from Probe A, Probe B observed a clear increase of the normal angles of whistler waves after the substorm injection, which can also be identified in Figure 11 on a relatively longer timescale. The precise physical process responsible for the normal angle variation of both chorus and exohiss waves remains unclear. One possibility is the change of the wave propagation paths associated with the geomagnetic field reconfiguration during the substorm.

3.2 Simulation

We next examine whether substorm-injected electrons could amplify the exohiss waves through cyclotron resonance at the equator. Around the substorm injection, the twin probes were located at the magnetic latitudes of -12° . The equatorial cold electron number density N_0 and phase space density F are assumed to equal those observed locally. Figure 4 plots the observed and modeled hot electron phase space densities dependent on energy E_k and pitch angle α before and after the substorm injection. Before the substorm injection, the hot electron phase space density function is written as a combination of three subtracted Max-

wellian components (Ashour-Abdalla and Kennel, 1978):

$$F = \sum_{i=1}^3 F_i = \sum_{i=1}^3 \frac{n_i}{\sqrt{\pi} \mu_{\parallel i} \mu_{\perp i}} \exp\left(\frac{-v_{\parallel}^2}{\mu_{\parallel i}^2}\right) \times \left\{ \sigma_i \exp\left(\frac{-v_{\perp}^2}{\mu_{\perp i}^2}\right) + \frac{1 - \sigma_i}{1 - \beta_i} \left[\exp\left(\frac{-v_{\perp}^2}{\mu_{\perp i}^2}\right) - \exp\left(\frac{-v_{\perp}^2}{\beta_i \mu_{\perp i}^2}\right) \right] \right\}, \quad (3)$$

with density parameter n_i , thermal parameters $\mu_{\perp i}$ and $\mu_{\parallel i}$, and loss cone parameters σ_i and β_i of each component. After the substorm injection, the two low energy components are assumed to be unchanged. To reproduce the phase space density peak near $E_k = 100 \text{ keV}$, the third component is expressed as

$$F_3 = \rho \left(\sin^{\zeta} \alpha + \epsilon \right) \exp\left[-\left(\frac{v - \mu}{\tau}\right)^2\right], \quad (4)$$

with density-like parameter ρ , thermal parameters μ and τ , and loss cone parameters ζ and ϵ . All these fitting parameters before and after the substorm injection are listed in Table 1. Clearly, the modeled and observed electron phase space densities agree reasonably well with each other for both probes.

Figure 5 shows the wave growth rates and spectral densities before and after the substorm injection. According to the observa-

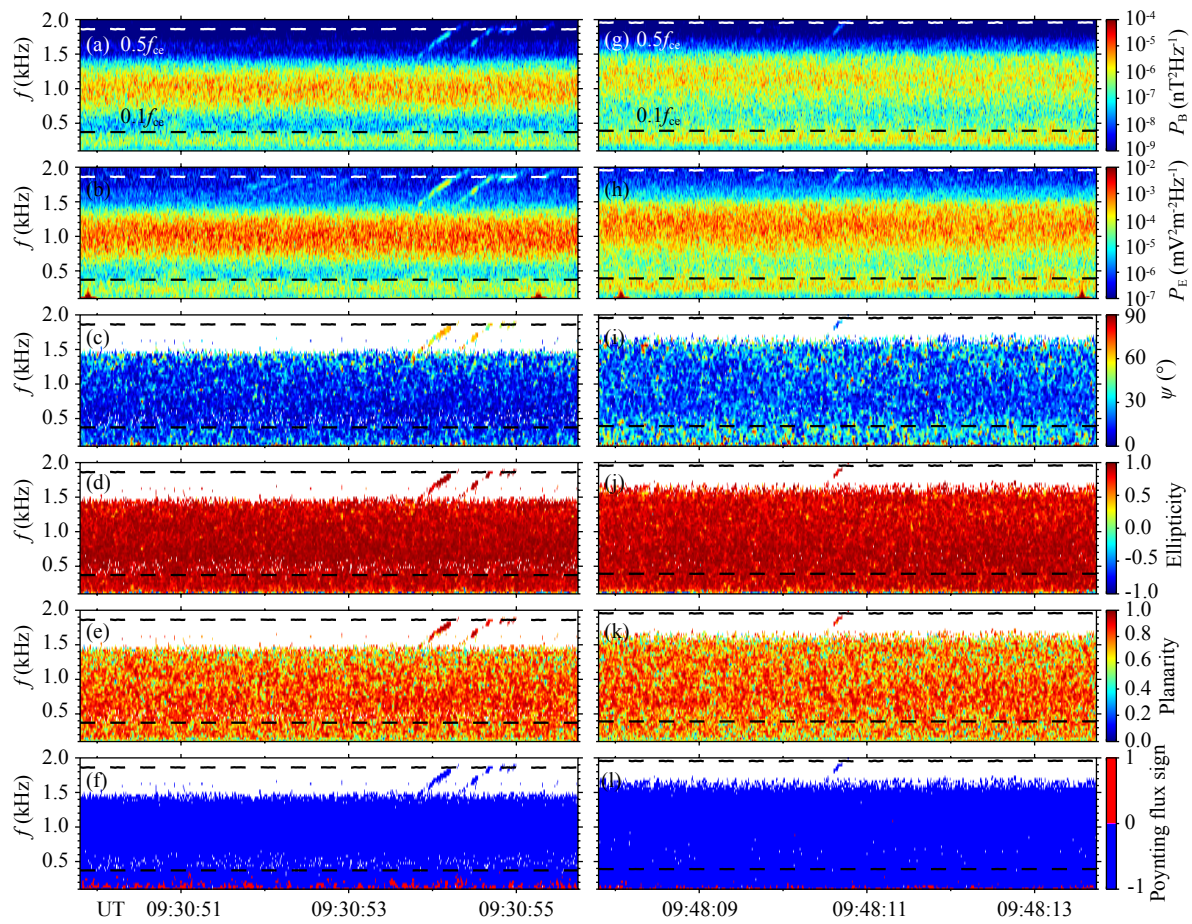


Figure 3. Same as Figure 2 but for Probe B.

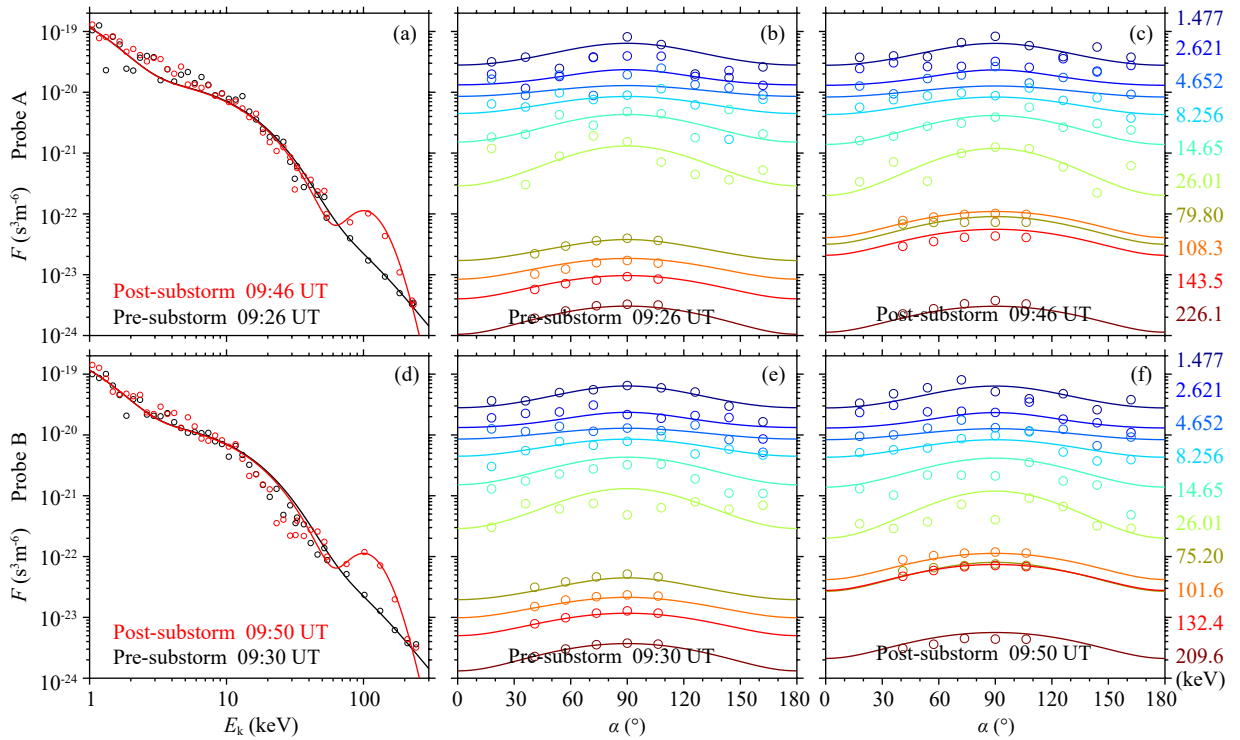


Figure 4. Observed (circles) and modeled (lines) electron phase space densities for Van Allen Probes A (a–c) and B (d–f): (a, d) energy-dependent profiles at the pitch angle $\alpha = 90^\circ$; (b, c, e, f) pitch-angle-dependent profiles at the selected energies.

Table 1. Fitting Parameters for electron phase space density

		n_i (m^{-3})	$\mu_{\perp i}$ (ms^{-1})	$\mu_{\parallel i}$ (ms^{-1})	σ_i	β_i
Low energy	pre & post	7×10^3	1.5×10^7	1.2×10^7	1.00	0.9
		15×10^3	5×10^7	4.3×10^7	0.8	0.9
High energy	pre	n_i (m^{-3})	$\mu_{\perp i}$ (ms^{-1})	$\mu_{\parallel i}$ (ms^{-1})	σ_i	β_i
		1.4×10^3	9.6×10^7	9.3×10^7	0.8	0.9
	post	ρ ($\text{s}^3 \text{m}^{-6}$)	μ (ms^{-1})	τ (ms^{-1})	ζ	ϵ
		7×10^{-23}	1.65×10^8	2.7×10^7	2.0	0.6

tions in Figures 1e and 2c, the linear instabilities of parallel-propagating whistler waves are analyzed for Probe A. Before the substorm injection, the most pronounced peak of the growth rate occurs in the chorus band centering at $f/f_{ce} = 0.25$. After the substorm injection, the modeled electron phase space densities below $E_k < 60$ keV are unchanged (Figure 4) and the magnitudes of wave growth rates in the frequency range $f/f_{ce} = 0.15–0.37$ increase slightly, roughly explaining the insignificant variation of the power spectral densities in the chorus band. In contrast, the enhancement of electron phase space densities above $E_k > 60$ keV produces a new peak ($1.1 \times 10^{-7} \text{ m}^{-1}$) of wave growth rate in the

frequency range $0.03–0.1f_{ce}$. According to the linear theory, the preexisting exohiss lying in the frequency range below $0.1f_{ce}$ should experience an amplification. Assuming that the exohiss amplification occurs within 10° latitude of the magnetic equatorial plane (with the magnetic field line length $s \sim 1.3 \times 10^7 \text{ m}$) and that the wave growth rates are constant ($K_i \sim 10^{-7} \text{ m}^{-1}$), we can roughly obtain the path-integrated amplification ratio of exohiss power $\bar{P} = \frac{P_f}{P_i} = [\exp(K_i s)]^2 = 13.4$ (with final wave power P_f and initial wave power P_i). The simulated amplification generally explains the observed intensification (up to 10 times) of exohiss power spectral densities. Considering the observed normal angle

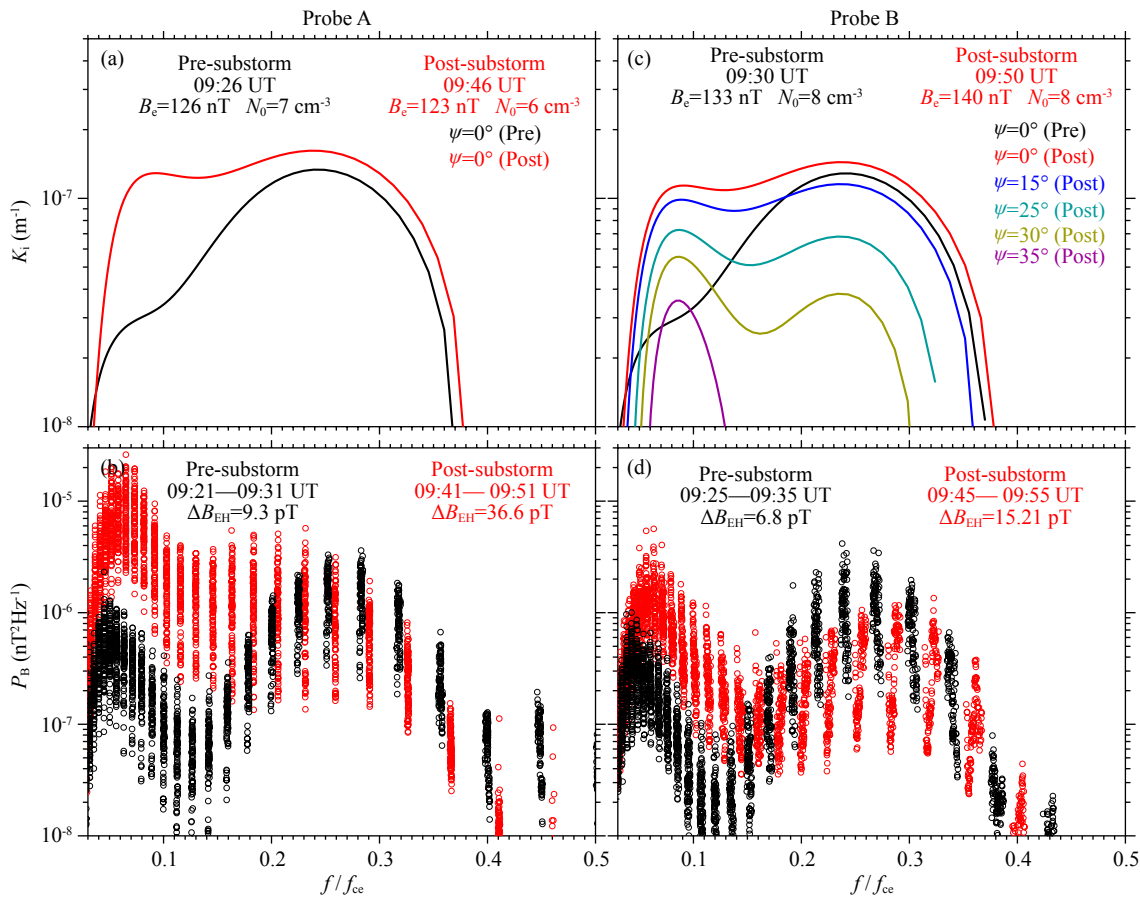


Figure 5. Convective growth rates (a, c) and magnetic power spectral densities (b, d) of whistler-mode waves for Van Allen Probes A (left) and B (right). Equatorial magnetic field B_e and cold electron density N_0 for calculations are listed in Figures 5a and 5c. The averaged amplitudes of exohiss ΔB_{EH} before and after the substorm injection are listed in Figures 5b and 5d. Convective growth rates are color-coded according to normal angles and time (shown).

variations for Probe B (Figures 11 and 3i), we have calculated the wave linear growth rates at normal angles of 0° , 15° , 25° , 30° and 35° , respectively. One can find that, for the whistler wave with a larger normal angle, the frequency range allowing wave growth becomes narrower, and the corresponding peak growth rates become lower. Because of the increase of exohiss wave normal angle after the substorm injection (Figures 11 and 3i), Probe B observed a weaker enhancement of wave power than Probe A. The wave growth rates at larger normal angles exhibit a more obvious gap between exohiss and chorus bands, explaining the merged quasi-parallel bands of RBSP-A and the split oblique bands of RBSP-B.

Considering the temporal evolution of injected electron fluxes, we analyze the dynamic instabilities of whistler waves over a time period to give a more comprehensive view of exohiss amplification. As shown in Figure 5, the exohiss is amplified mainly by energetic (> 60 keV) electrons. We use the smooth cubic spline ap-

proximation (Reinsch, 1967) to model the electron phase space density observed by MagEIS (> 30 keV) and adopt the B-spline interpolation (De Boor, 1977) to evaluate the required partial derivative of the electron phase space density with respect to the velocity vector (more details given by Liu NG et al., 2018a). In Figure 6, one can observe clear correlations between enhancements in the observed wave power and in the calculated growth rates of exohiss waves. The obtained growth rates appear to be quite small (10^{-8} – 10^{-7} m $^{-1}$), suggesting that it is difficult for energetic electrons alone (without preexisting source waves) to produce observable whistler waves. However, when wave growth is allowed in the frequency range of < 400 Hz, the preexisting exohiss can be effectively amplified. After 09:50 UT, the peak frequency of the wave growth rate increases rapidly, accounting for the observed frequency variation of exohiss waves. The main cause is the rapid decrease of the upper energy cut-off of the substorm-injected electrons. Corresponding to the observed weakening of wave

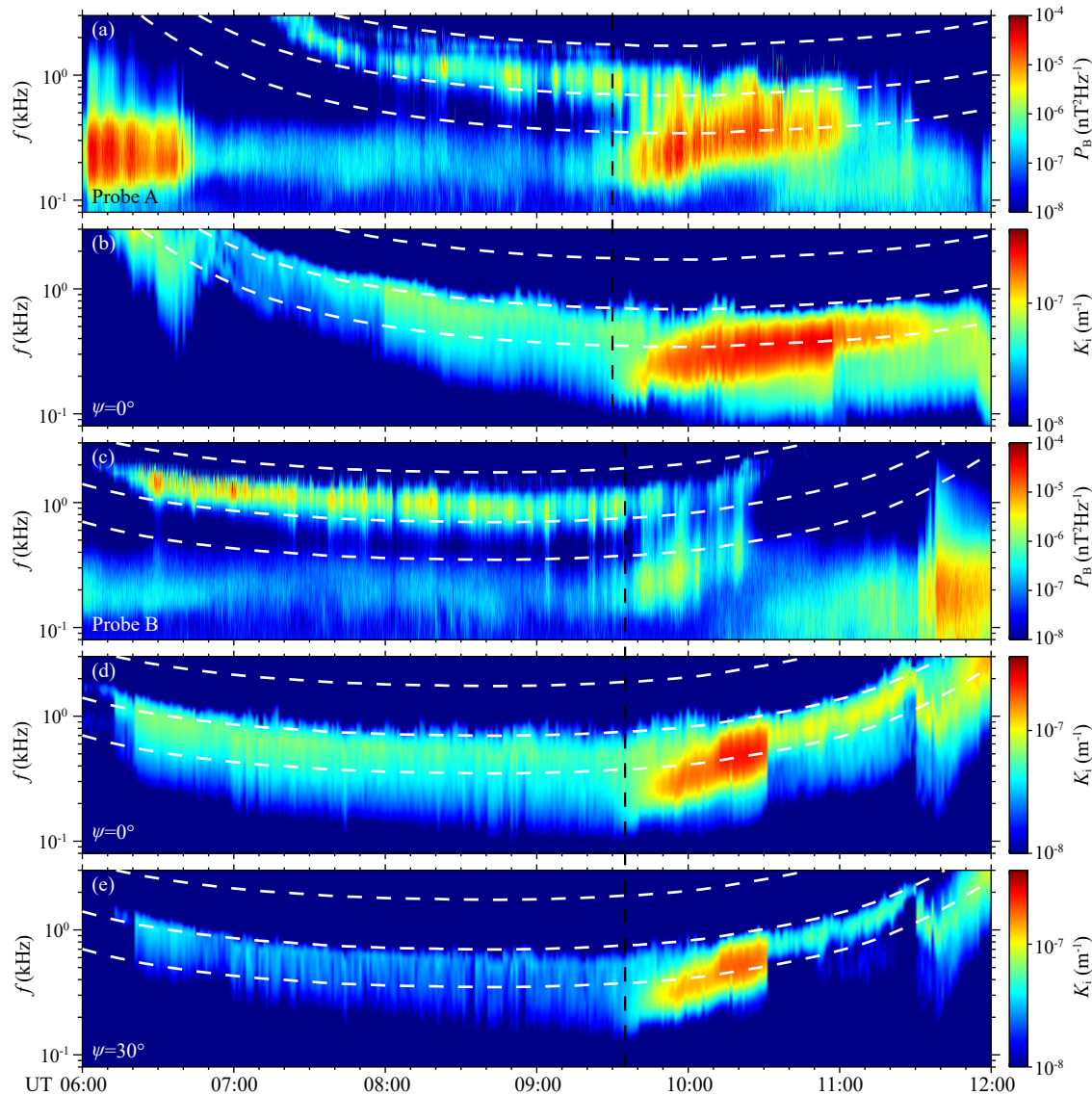


Figure 6. Variations of wave power P_B (a, c) and convective growth rate K_i (b, d, e) for whistler-mode waves around the substorm event on 21 February 2014. Dashed lines in each figure represent 0.1, 0.2, and 0.5 f_{ce} . The vertical black lines mark the arrival time of the substorm injection.

power for Probe A after 10:55 UT and for Probe B after 10:30 UT, the calculated growth rates decrease significantly because of the reduction of electron temperature anisotropy.

4. Event on 5 May 2014

To illustrate the generality of the previously obtained results, we additionally show an exohiss amplification event observed by the Van Allen Probes on 5 May 2014. An overview of this event is given in Figure 7; the wave fine structure of Probe B before and after

the substorm injection is given in Figure 8. The propagation characteristics of plasmaspheric hiss, chorus, and exohiss were quite similar to those of the previous event on 21 February 2014. Outside the plasmapause, both the exohiss and the lower band chorus appeared to be structureless, while some rising tones constituted the upper band chorus. Around 07:30, the chorus exhibited a reversion in the direction of Poynting flux across the equator, indicating its equatorial generation (Santolík et al., 2003b). In contrast, the exohiss leaked out of the high-latitude plasmapause (Thorne et al., 1973) had bi-directional Poynting flux near the

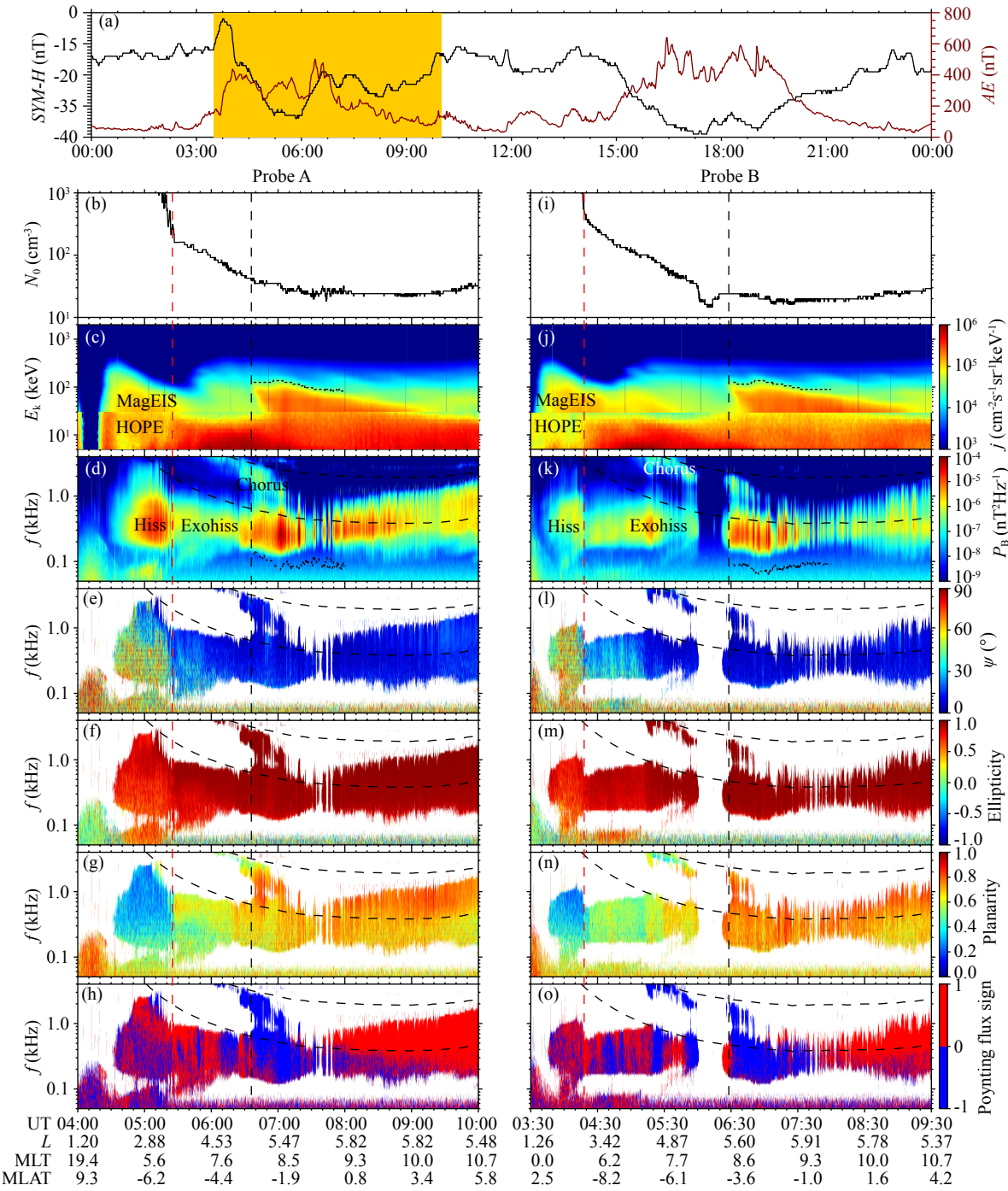


Figure 7. Same as Figure 1 except for the 5 May 2014 event. In the time range of 06:00–06:15 UT, Van Allen Probe B detected no clear chorus and exohiss waves, probably associated with the low-density trough structure.

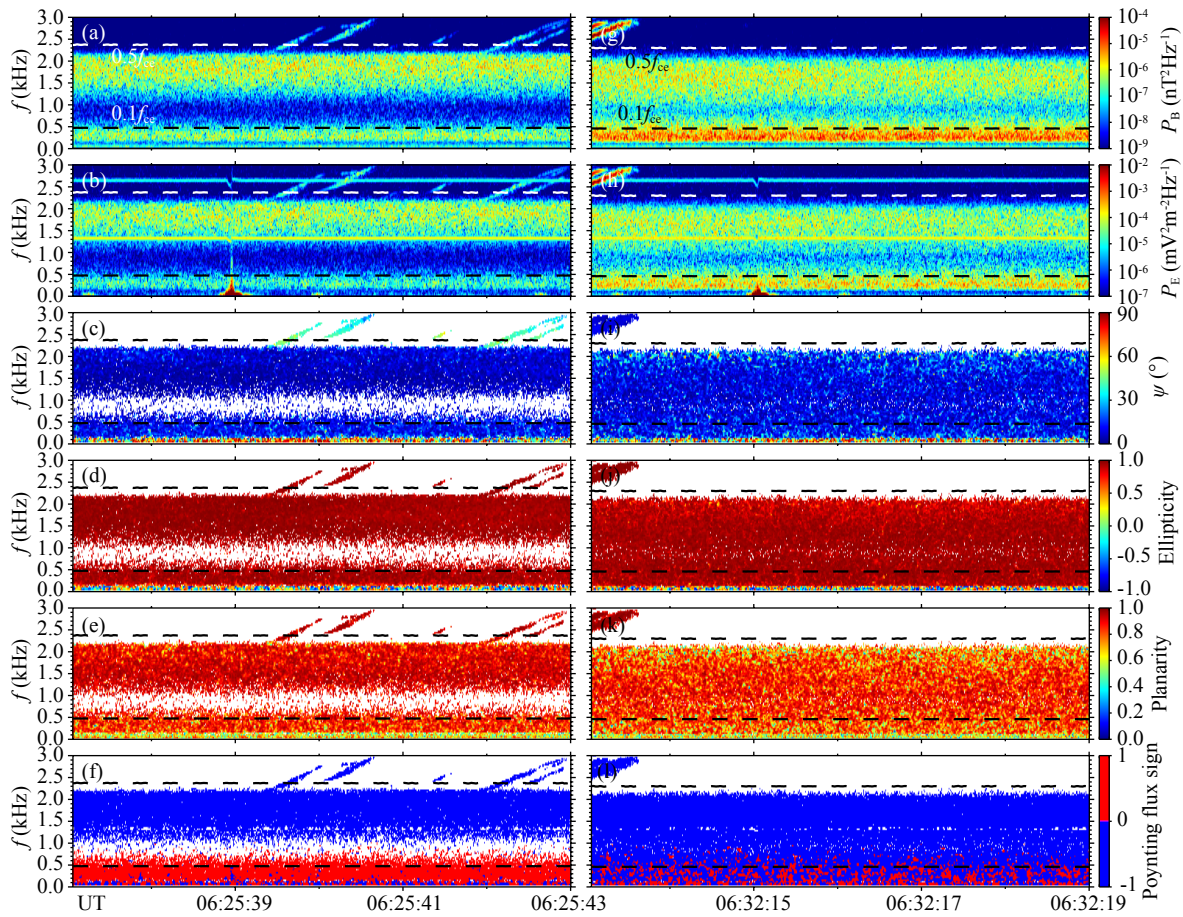


Figure 8. Same as Figure 2 except for the 5 May 2014 event recorded by Van Allen Probe B.

equator (Zhu H et al., 2015). The substorm injection was detected by the twin Van Allen Probes around 06:35 UT in the dayside (MLT \sim 08:00–09:00) equatorial region at $L \sim 5$ –6. The upper energy cut-offs of the substorm injection were \sim < 200 keV, and the corresponding minimum cyclotron resonant frequencies were well below the lower frequency cut-offs of the exohiss waves. After the substorm injection, the exohiss waves were obviously intensified (up to 10 times, at the location of Probe B). Using the MagEIS data (>30 keV), we calculate the linear growth rates of parallel-propagating whistler waves (Figure 9). Just after the substorm injection, the modeled growth rates peak around 600 Hz for Probe A, producing relatively limited effect on exohiss in the frequency range of 100–500 Hz. About 20 min later, the decreased background magnetic field allows the growth of waves at lower frequencies, corresponding to the significant enhancement of exohiss waves observed by Probe A. In contrast, Probe B encountered the substorm injection at an outer L -shell with a weaker background magnetic field and then observed a prompt enhancement of exohiss after the substorm injection. These results support the conclusion that substorm injected energetic electrons amplify exohiss.

5. Summary

Generation and evolution of whistler-mode chorus and plasmaspheric hiss have attracted considerable attention in past dec-

ades. In this study, we focus on the evolution of a poorly-understood whistler-mode emission outside the plasmasphere named exohiss (Thorne et al., 1973). On 21 February 2014, the twin Van Allen Probes detected a substorm injection in the noonside (MLT \sim 12:00–13:00) southern hemisphere ($MLAT < -10^\circ$) outside the plasmasphere ($L = 6.0$). In response to the sudden enhancement of 60–200 keV energetic electron fluxes by up to 5 times, the power spectral densities of exohiss waves exhibited intensification of up to 10 times. The linear instability of energetic electrons (Kennel, 1966; Chen LJ et al., 2010) is shown to be able to generally explain the timing and the magnitude of exohiss wave enhancement. Before the substorm injection, the growth rates are found to peak in the chorus band (0.1–0.5 f_{ce}). The substorm-injected energetic electrons are able to produce a new peak of growth rate in the exohiss band (< 0.1 f_{ce}). The corresponding peak growth rate is about 10^{-7} m^{-1} and the path-integrated amplification rate of wave power within 10° latitude of the magnetic equatorial plane reaches $\bar{P} = 13.4$. The analogous evolution characteristics of exohiss were also observed by Van Allen Probes on 5 May 2014. These data and modeling tend to support the amplification of exohiss, probably originating from the plasmaspheric hiss, by substorm-injected energetic electrons.

It should be mentioned that this study is limited to simple analyses of some local plasma instabilities. More rigorous future testing of the exohiss amplification scenario should be done with ray-

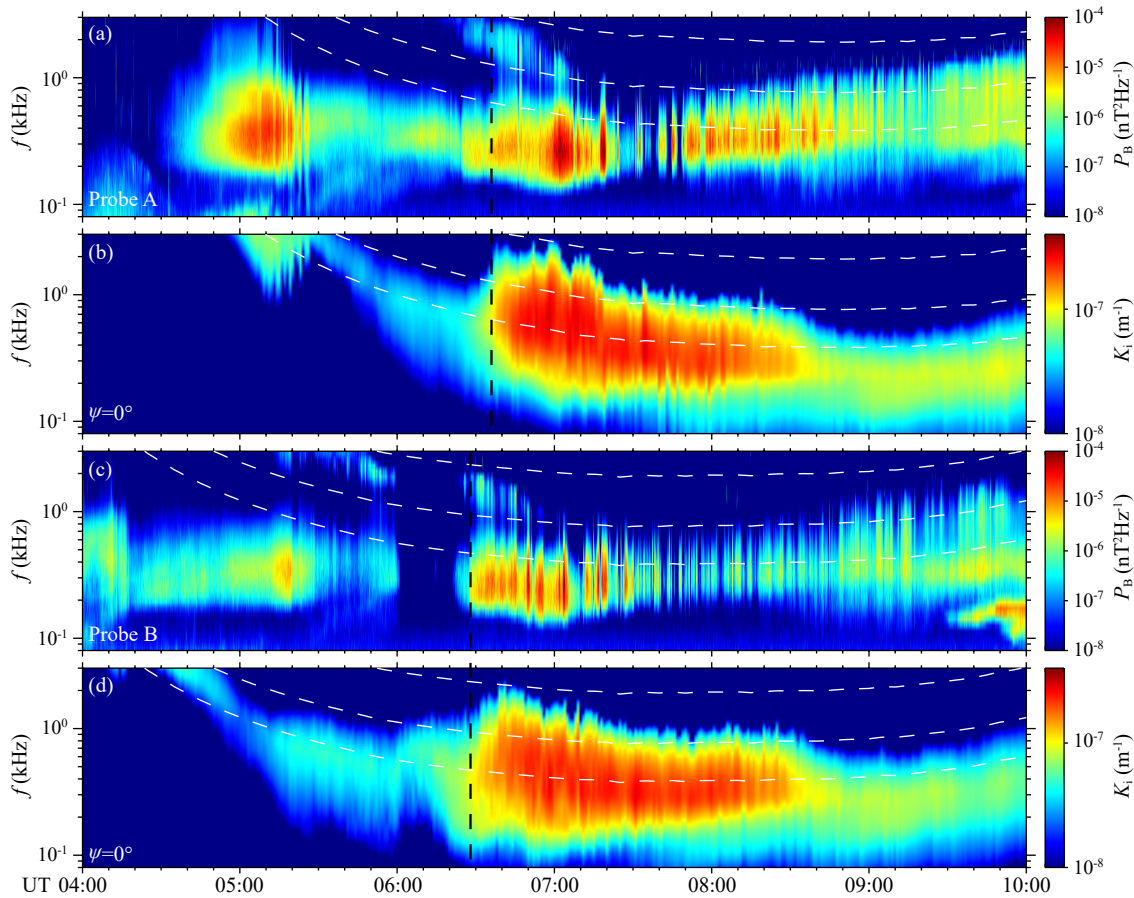


Figure 9. Same as Figure 6 except for the 5 May 2014 event.

tracing simulations (e.g., Horne, 1989) and/or particle simulations. For the events reported here, the substorms caused the exohiss amplitude to increase from <10 pT to ~40 pT. Future studies should investigate the statistical characteristics of exohiss and adopt some global models (e.g., Varotsou et al., 2008; Albert et al., 2009; Shprits et al., 2009; Su ZP et al., 2010, 2011; Tu WC et al., 2014) to accurately evaluate the role of exohiss waves in radiation belt electron dynamics.

Acknowledgments

This work was supported by National Natural Science Foundation of China grants 41631071, 41774170, 41274174, 41174125, 41131065, 41421063, 41231066 and 41304134, Chinese Academy of Sciences grants KZCX2-EW-QN510 and KZZD-EW-01-4, CAS Key Research Program of Frontier Sciences grant QYZDB-SSW-DQC015, National Key Basic Research Special Foundation of China Grant No. 2011CB811403, and Fundamental Research Funds for the Central Universities WK2080000077. We acknowledge the University of Iowa as the source of EMFISIS data (this acknowledgement does not imply endorsement of the publication by the University of Iowa or its researchers). The Van Allen Probes data are available at the websites: EMFISIS, <http://emfisis.physics.uiowa.edu/Flight/>, ECT, <http://www.rbsp-ect.lanl.gov/datapub/>.

References

Abel, B., and Thorne, R. M. (1998). Electron scattering loss in Earth's inner

magnetosphere: 1. Dominant physical processes. *Geophys. J. Res.*, 103(A2), 2385–2396. <https://doi.org/10.1029/97JA02919>

Albert, J. M., Meredith, N. P., and Horne, R. B. (2009). Three-dimensional diffusion simulation of outer radiation belt electrons during the 9 October 1990 magnetic storm. *J. Geophys. Res.*, 114(9), A09214. <https://doi.org/10.1029/2009JA014336>

Artemyev, A., Agapitov, O., Breuillard, H., Krasnoselskikh, V., and Rolland, G. (2012). Electron pitch-angle diffusion in radiation belts: The effects of whistler wave oblique propagation. *Geophys. Res. Lett.*, 39(8), L08105. <https://doi.org/10.1029/2012GL051393>

Ashour-Abdalla, M., and Kennel, C. F. (1978). Nonconvective and convective electron cyclotron harmonic instabilities. *J. Geophys. Res.*, 83(A4), 1531–1543. <https://doi.org/10.1029/JA083iA04p01531>

Blake, J. B., Carranza, P. A., Claudepierre, S. G., Clemons, J. H., Crain, W. R. Jr., Dotan, Y., Fennell, J. F., Fuentes, F. H., Galvan, R. M., ... Zakrzewski, M. P. (2013). The magnetic electron ion spectrometer (MagEIS) instruments aboard the radiation belt storm probes (RBSP) spacecraft. *Space Sci. Rev.*, 179(1–4), 383–421. <https://doi.org/10.1007/s11214-013-9991-8>

Bortnik, J., Thorne, R. M., and Meredith, N. P. (2008). The unexpected origin of plasmaspheric hiss from discrete chorus emissions. *Nature*, 452(7183), 62–66. <https://doi.org/10.1038/nature06741>

Bortnik, J., Li, W., Thorne, R. M., Angelopoulos, V., Cully, C., Bonnell, J., Le Contel, C., and Roux, A. (2009). An observation linking the origin of plasmaspheric hiss to discrete chorus emissions. *Science*, 324(5928), 775–778. <https://doi.org/10.1126/science.1171273>

Cattell, C. A., Breneman, A. W., Thaller, S. A., Wygant, J. R., Kletzing, C., and Kurth, W. S. (2015). Van Allen Probes observations of unusually low frequency whistler mode waves observed in association with moderate magnetic storms: Statistical study. *Geophys. Res. Lett.*, 42(18), 7273–7281. <https://doi.org/10.1002/2015GL065565>

- Chen, L. J., Thorne, R. M., Jordanova, V. K., and Horne, R. B. (2010). Global simulation of magnetosonic wave instability in the storm time magnetosphere. *J. Geophys. Res.*, 115(A11), A11222. <https://doi.org/10.1029/2010JA015707>
- Chen, L. J., Thorne, R. M., Bortnik, J., Li, W., Horne, R. B., Reeves, G. D., Kletzing, C. A., Kurth, W. S., Hospodarsky, G. B., ... Fennell, J. F. (2014). Generation of unusually low frequency plasmaspheric hiss. *Geophys. Res. Lett.*, 41(16), 5702–5709. <https://doi.org/10.1002/2014GL060628>
- De Boor, C. (1977). Package for calculating with B-Splines. *SIAM J. Numer. Anal.*, 14(3), 441–472. <https://doi.org/10.1137/0714026>
- Funsten, H. O., Skoug, R. M., Guthrie, A. A., MacDonald, E. A., Baldonado, J. R., Harper, R. W., Henderson, K. C., Kihara, K. H., ... Chen, J. (2013). Helium, Oxygen, Proton, and Electron (HOPE) mass spectrometer for the radiation belt storm probes mission. *Space Sci. Rev.*, 179(1–4), 423–484. <https://doi.org/10.1007/s11214-013-9968-7>
- Gao, Z. L., Su, Z. P., Zhu, H., Xiao, F. L., Zheng, H. N., Wang, Y. M., Shen, C., and Wang, S. (2016). Intense low-frequency chorus waves observed by Van Allen Probes: Fine structures and potential effect on radiation belt electrons. *Geophys. Res. Lett.*, 43(3), 967–977. <https://doi.org/10.1002/2016GL067687>
- Golden, D. I., Spasojevic, M., and Inan, U. S. (2009). Diurnal dependence of ELF/VLF hiss and its relation to chorus at $L = 2.4$. *J. Geophys. Res.*, 114(A5), A05212. <https://doi.org/10.1029/2008JA013946>
- Golden, D. I., Spasojevic, M., and Inan, U. S. (2011). Determination of solar cycle variations of midlatitude ELF/VLF chorus and hiss via automated signal detection. *J. Geophys. Res.*, 116(A3), A03225. <https://doi.org/10.1029/2010JA016193>
- Green, J. L., Boardsen, S., Garcia, L., Taylor, W. W. L., Fung, S. F., and Reinsch, B. W. (2005). On the origin of whistler mode radiation in the plasmasphere. *J. Geophys. Res.*, 110(A3), A03201. <https://doi.org/10.1029/2004JA010495>
- Horne, R. B. (1989). Path-integrated growth of electrostatic waves: The generation of terrestrial myriametric radiation. *J. Geophys. Res.*, 94(A7), 8895–8909. <https://doi.org/10.1029/JA094iA07p08895>
- Horne, R. B., and Thorne, R. M. (1998). Potential waves for relativistic electron scattering and stochastic acceleration during magnetic storms. *Geophys. Res. Lett.*, 25(15), 3011–3014. <https://doi.org/10.1029/98GL01002>
- Horne, R. B., Thorne, R. M., Shprits, Y. Y., Meredith, N. P., Glauert, S. A., Smith, A. J., Kanekal, S. G., Baker, D. N., Engebretson, M. J., ... Decreau, P. M. E. (2005). Wave acceleration of electrons in the Van Allen radiation belts. *Nature*, 437(7056), 227–230. <https://doi.org/10.1038/nature03939>
- Kennel, C. (1966). Low-frequency whistler mode. *Phys. Fluids*, 9(11), 2190–2202. <https://doi.org/10.1063/1.1761588>
- Kennel, C. F., and Engelmann, F. (1966). Velocity space diffusion from weak plasma turbulence in a magnetic field. *Phys. Fluids*, 9(12), 2377–2388. <https://doi.org/10.1063/1.1761629>
- Kletzing, C. A., Kurth, W. S., Acuna, M., MacDowall, R. J., Torbert, R. B., Averkamp, T., Bodet, D., Bounds, S. R., Chutter, M., ... Tyler, J. (2013). The electric and magnetic field instrument suite and integrated science (EMFISIS) on RBSP. *Space Sci. Rev.*, 179(1–4), 127–181. <https://doi.org/10.1007/s11214-013-9993-6>
- Kurth, W. S., and Gurnett, D. A. (1991). Plasma waves in planetary magnetospheres. *J. Geophys. Res.*, 96(S01), 18977–18991. <https://doi.org/10.1029/91JA01819>
- Kurth, W. S., De Pascuale, S., Faden, J. B., Kletzing, C. A., Hospodarsky, G. B., Thaller, S., and Wygant, J. R. (2014). Electron densities inferred from plasma wave spectra obtained by the waves instrument on Van Allen Probes. *J. Geophys. Res.*, 120(2), 904–914. <https://doi.org/10.1002/2014JA020857>
- Li, W., Thorne, R. M., Angelopoulos, V., Bonnell, J. W., McFadden, J. P., Carlson, C. W., LeContel, O., Roux, A., Glassmeier, K. H., and Auster, H. U. (2009). Evaluation of whistler-mode chorus intensification on the nightside during an injection event observed on the THEMIS spacecraft. *J. Geophys. Res.*, 114(A1), A00C14. <https://doi.org/10.1029/2008JA013554>
- Li, W., Thorne, R. M., Bortnik, J., Reeves, G. D., Kletzing, C. A., Kurth, W. S., Hospodarsky, G. B., Spence, H. E., Blake, J. B., ... Thaller, S. A. (2013). An unusual enhancement of low-frequency plasmaspheric hiss in the outer plasmasphere associated with substorm-injected electrons. *Geophys. Res. Lett.*, 40(15), 3798–3803. <https://doi.org/10.1002/grl.50787>
- Liu, N. G., Su, Z. P., Gao, Z. L., Zheng, H. N., Wang, Y. M., Wang, S., Spence, H. E., Reeves, G. D., Baker, D. N., ... Wygant, J. R. (2017). Simultaneous disappearances of plasmaspheric hiss, exohiss, and chorus waves triggered by a sudden decrease in solar wind dynamic pressure. *Geophys. Res. Lett.*, 44(1), 52–61. <https://doi.org/10.1002/2016GL071987>
- Liu, N. G., Su, Z. P., Zheng, H. N., Wang, Y. M., and Wang, S. (2018a). Prompt disappearance and emergence of radiation belt magnetosonic waves induced by solar wind dynamic pressure variations. *Geophys. Res. Lett.*, 45(2), 585–594. <https://doi.org/10.1002/2017GL076382>
- Liu, N. G., Su, Z. P., Zheng, H. N., Wang, Y. M., and Wang, S. (2018b). Magnetosonic harmonic falling and rising frequency emissions potentially generated by nonlinear wave-wave interactions in the Van Allen radiation belts. *Geophys. Res. Lett.* <https://doi.org/10.1029/2018GL079232>
- Mauk, B. H., Fox, N. J., Kanekal, S. G., Kessel, R. L., Sibeck, D. G., and Ukhorskiy, A. (2013). Science objectives and rationale for the radiation belt storm probes mission. *Space Sci. Rev.*, 179(1–4), 3–27. <https://doi.org/10.1007/s11214-012-9908-y>
- Ni, B. B., Li, W., Thorne, R. M., Bortnik, J., Ma, Q. L., Chen, L. J., Kletzing, C. A., Kurth, W. S., Hospodarsky, G. B., ... Claudepiere, S. G. (2014). Resonant scattering of energetic electrons by unusual low-frequency hiss. *Geophys. Res. Lett.*, 41(6), 1854–1861. <https://doi.org/10.1002/2014GL059389>
- Nunn, D., Omura, Y., Matsumoto, H., Nagano, I., and Yagitani, S. (1997). The numerical simulation of VLF chorus and discrete emissions observed on the Geotail satellite using a Vlasov code. *J. Geophys. Res.*, 102(A12), 27083–27098. <https://doi.org/10.1029/97JA02518>
- Omura, Y., Katoh, Y., and Summers, D. (2008). Theory and simulation of the generation of whistler-mode chorus. *J. Geophys. Res.*, 113(A4), A04223. <https://doi.org/10.1029/2007JA012622>
- Reinsch, C. H. (1967). Smoothing by spline functions. *Numer. Mathem.*, 10(3), 177–183. <https://doi.org/10.1007/BF02162161>
- Russell, C. T., Holzer, R. E., and Smith, E. J. (1969). OGO 3 observations of ELF noise in the magnetosphere: 1. Spatial extent and frequency of occurrence. *J. Geophys. Res.*, 74(3), 755–777. <https://doi.org/10.1029/JA074i003p00755>
- Santolík, O., Pickett, J. S., Gurnett, D. A., and Storey, L. R. O. (2002). Magnetic component of narrowband ion cyclotron waves in the auroral zone. *J. Geophys. Res.*, 107(A12), SMP 17-1–SMP 17-14. <https://doi.org/10.1029/2001JA000146>
- Santolík, O., Parrot, M., and Lefevre, F. (2003a). Singular value decomposition methods for wave propagation analysis. *Radio Sci.*, 38(1), 1010. <https://doi.org/10.1029/2000RS002523>
- Santolík, O., Gurnett, D. A., Pickett, J. S., Parrot, M., and Cornilleau-Wehrlin, N. (2003b). Spatio-temporal structure of storm-time chorus. *J. Geophys. Res.*, 108(A7), 1278. <https://doi.org/10.1029/2002JA009791>
- Santolík, O., Pickett, J. S., Gurnett, D. A., Menietti, J. D., Tsurutani, B. T., and Verkhoglyadova, O. (2010). Survey of Poynting flux of whistler mode chorus in the outer zone. *J. Geophys. Res.*, 115(A7), A00F13. <https://doi.org/10.1029/2009JA014925>
- Santolík, O., Kletzing, C. A., Kurth, W. S., Hospodarsky, G., and Bounds, S. R. (2014). Fine structure of large-amplitude chorus wave packets. *Geophys. Res. Lett.*, 41(2), 293–299. <https://doi.org/10.1002/2013GL058889>
- Shprits, Y. Y., Thorne, R. M., Horne, R. B., Glauert, S. A., Cartwright, M., Russell, C. T., Baker, D. N., and Kanekal, S. G. (2006). Acceleration mechanism responsible for the formation of the new radiation belt during the 2003 Halloween solar storm. *Geophys. Res. Lett.*, 33(5), L05104. <https://doi.org/10.1029/2005GL024256>
- Shprits, Y. Y., Subbotin, D., and Ni, B. B. (2009). Evolution of electron fluxes in the outer radiation belt computed with the VERB code. *J. Geophys. Res.*, 114(A11), A11209. <https://doi.org/10.1029/2008JA013784>
- Solomon, J., Cornilleau-Wehrlin, N., Korth, A., and Kremser, G. (1988). An experimental study of ELF/VLF hiss generation in the earth's magnetosphere. *J. Geophys. Res.*, 93(A3), 1839–1847. <https://doi.org/10.1029/JA093iA03p01839>
- Sonwalkar, V. S., and Inan, U. S. (1989). Lightning as an embryonic source of VLF hiss. *J. Geophys. Res.*, 94(A6), 6986–6994. <https://doi.org/10.1029/JA094iA06p06986>
- Spence, H. E., Reeves, G. D., Baker, D. N., Blake, J. B., Bolton, M., Bourdarie, S.,

- Chan, A. A., Claudepierre, S. G., Clemmons, J. H., ... Thorne, R. M. (2013). Science goals and overview of the radiation belt storm probes (RBSP) energetic particle, composition, and thermal plasma (ECT) suite on NASA's Van Allen probes mission. *Space Sci. Rev.*, 179(1-4), 311–336.
<https://doi.org/10.1007/s11214-013-0007-5>
- Su, Z. P., Xiao, F. L., Zheng, H. N., and Wang, S. (2010). STEERB: A three-dimensional code for storm-time evolution of electron radiation belt. *J. Geophys. Res.*, 115(A9), A09208. <https://doi.org/10.1029/2009JA015210>
- Su, Z. P., Xiao, F. L., Zheng, H. N., and Wang, S. (2011). Radiation belt electron dynamics driven by adiabatic transport, radial diffusion, and wave-particle interactions. *J. Geophys. Res.*, 116(A4), A04205.
<https://doi.org/10.1029/2010JA016228>
- Su, Z. P., Xiao, F. L., Zheng, H. N., He, Z. G., Zhu, H., Zhang, M., Shen, C., Wang, Y. M., Wang, S., ... Baker, D. N. (2014a). Nonstorm time dynamics of electron radiation belts observed by the Van Allen Probes. *Geophys. Res. Lett.*, 41(2), 229–235. <https://doi.org/10.1002/2013GL058912>
- Su, Z. P., Zhu, H., Xiao, F. L., Zheng, H. N., Wang, Y. M., He, Z. G., Shen, C., Shen, C. L., Wang, C. B., ... Wygant, J. R. (2014b). Intense duskside lower band chorus waves observed by Van Allen Probes: Generation and potential acceleration effect on radiation belt electrons. *J. Geophys. Res.*, 119(6), 4266–4273.
<https://doi.org/10.1002/2014JA019919>
- Su, Z. P., Zhu, H., Xiao, F. L., Zheng, H. N., Wang, Y. M., Shen, C., Zhang, M., Wang, S., Kletzing, C. A., ... Wygant, J. R. (2015). Disappearance of plasmaspheric hiss following interplanetary shock. *Geophys. Res. Lett.*, 42(9), 3129–3140.
<https://doi.org/10.1002/2015GL063906>
- Su, Z. P., Gao, Z. L., Zhu, H., Li, W., Zheng, H. N., Wang, Y. M., Wang, S., Spence, H. E., Reeves, G. D., ... Wygant, J. R. (2016). Nonstorm time dropout of radiation belt electron fluxes on 24 September 2013. *J. Geophys. Res.*, 121(7), 6400–6416. <https://doi.org/10.1002/2016JA022546>
- Su, Z. P., Liu, N. G., Zheng, H. N., Wang, Y. M., and Wang, S. (2018). Large-amplitude extremely low frequency hiss waves in plasmaspheric plumes. *Geophys. Res. Lett.*, 45(2), 565–577. <https://doi.org/10.1002/2017GL076754>
- Summers, D., Thorne, R. M., and Xiao, F. L. (1998). Relativistic theory of wave-particle resonant diffusion with application to electron acceleration in the magnetosphere. *J. Geophys. Res.*, 103(A9), 20487–20500.
<https://doi.org/10.1029/98JA01740>
- Summers, D., Ma, C., Meredith, N. P., Horne, R. B., Thorne, R. M., Heynderickx, D., and Anderson, R. R. (2002). Model of the energization of outer-zone electrons by whistler-mode chorus during the October 9, 1990 geomagnetic storm. *Geophys. Res. Lett.*, 29(24), 27-1–27-4.
<https://doi.org/10.1029/2002GL016039>
- Summers, D., Tong, R. S., and Thorne, R. M. (2009). Limit on stably trapped particle fluxes in planetary magnetospheres. *J. Geophys. Res.*, 114(A10), A10210. <https://doi.org/10.1029/2009JA014428>
- Summers, D., Omura, Y., Nakamura, S., and Kletzing, C. A. (2014). Fine structure of plasmaspheric hiss. *J. Geophys. Res.*, 119(11), 9134–9149.
<https://doi.org/10.1002/2014JA020437>
- Thorne, R. M., Smith, E. J., Burton, R. K., and Holzer, R. E. (1973). Plasmaspheric hiss. *J. Geophys. Res.*, 78(10), 1581–1596.
<https://doi.org/10.1029/JA078i010p01581>
- Thorne, R. M., Church, S. R., and Gorney, D. J. (1979). On the origin of plasmaspheric hiss: The importance of wave propagation and the plasmapause. *J. Geophys. Res.*, 84(A9), 5241–5247.
<https://doi.org/10.1029/JA084iA09p05241>
- Thorne, R. M. (2010). Radiation belt dynamics: The importance of wave-particle interactions. *Geophys. Res. Lett.*, 37(22), L22107.
<https://doi.org/10.1029/2010GL044990>
- Thorne, R. M., Li, W., Ni, B., Ma, Q., Bortnik, J., Chen, L., Baker, D. N., Spence, H. E., Reeves, G. D., ... Kanekal, S. G. (2013). Rapid local acceleration of relativistic radiation-belt electrons by magnetospheric chorus. *Nature*, 504(7480), 411–414. <https://doi.org/10.1038/nature12889>
- Tsyganenko, N. A., and Sitnov, M. I. (2005). Modeling the dynamics of the inner magnetosphere during strong geomagnetic storms. *J. Geophys. Res.*, 110(A3), A03208. <https://doi.org/10.1029/2004JA010798>
- Tu, W. C., Cunningham, G. S., Chen, Y., Morley, S. K., Reeves, G. D., Blake, J. B., Baker, D. N., and Spence, H. (2014). Event-specific chorus wave and electron seed population models in DREAM3D using the Van Allen Probes. *Geophys. Res. Lett.*, 41(5), 1359–1366. <https://doi.org/10.1002/2013GL058819>
- Varotsou, A., Boscher, D., Bourdarie, S., Horne, R. B., Meredith, N. P., Glauert, S. A., and Friedel, R. H. (2008). Three-dimensional test simulations of the outer radiation belt electron dynamics including electron-chorus resonant interactions. *J. Geophys. Res.*, 113(A12), A12212.
<https://doi.org/10.1029/2007JA012862>
- Yang, C., Su, Z. P., Xiao, F. L., Zheng, H. N., Wang, Y. M., Wang, S., Spence, H. E., Reeves, G. D., Baker, D. N., ... Funsten, H. O. (2016). Rapid flattening of butterfly pitch angle distributions of radiation belt electrons by whistler-mode chorus. *Geophys. Res. Lett.*, 43(16), 8339–8347.
<https://doi.org/10.1002/2016GL070194>
- Zhu, H., Su, Z. P., Xiao, F. L., Zheng, H. N., Wang, Y. M., Shen, C., Xian, T., Wang, S., Kletzing, C. A., ... Baker, D. N. (2015). Plasmatrough exohiss waves observed by Van Allen Probes: Evidence for leakage from plasmasphere and resonant scattering of radiation belt electrons. *Geophys. Res. Lett.*, 42(4), 1012–1019.
<https://doi.org/10.1002/2014GL062964>